

12

NOSC TD 721

NOSC TD 721

Technical Document 721

A RADAR SEA CLUTTER MODEL FOR ATMOSPHERIC DUCTING CONDITIONS

F. Perry Snyder
Marine Sciences and Technology Department

August 1984

Prepared for
Naval Air Systems Command

DTIC
SEP 07 1984

Approved for public release, distribution unlimited.

E

NOSC

NAVAL OCEAN SYSTEMS CENTER
San Diego, California 92152

84 09 06 033

AD-A145 321

DTIC FILE COPY



NAVAL OCEAN SYSTEMS CENTER SAN DIEGO, CA 92152

AN ACTIVITY OF THE NAVAL MATERIAL COMMAND

J.M. PATTON, CAPT, USN

Commander

R.M. HILLYER

Technical Director

ADMINISTRATIVE INFORMATION

The work discussed here was performed under program element 61153N (NOESC 532-MP07) for the Naval Air Systems Command. The work was performed between October 1979 and December 1983. This document was approved for publication 5 April 1984.

Released by
J. A. Ferguson
Modeling Branch

Under authority of
J. H. Richter, Head
Ocean and Atmospheric
Sciences Division

UNCLASSIFIED

SECURITY CLASSIFICATION OF THIS PAGE

REPORT DOCUMENTATION PAGE				
1a REPORT SECURITY CLASSIFICATION UNCLASSIFIED		1b RESTRICTIVE MARKINGS		
2a SECURITY CLASSIFICATION AUTHORITY		3 DISTRIBUTION/AVAILABILITY OF REPORT Approved for public release; distribution unlimited.		
2b DECLASSIFICATION/DOWNGRADING SCHEDULE		4 PERFORMING ORGANIZATION REPORT NUMBER(S) NOSC TD 721		
5 MONITORING ORGANIZATION REPORT NUMBER(S)		6a NAME OF PERFORMING ORGANIZATION Naval Ocean Systems Center		6b OFFICE SYMBOL (If applicable) Code 544
7a NAME OF MONITORING ORGANIZATION		6c ADDRESS (City, State and ZIP Code) San Diego, CA 92152		7b ADDRESS (City, State and ZIP Code)
8a NAME OF FUNDING/SPONSORING ORGANIZATION Naval Air Systems Command		8b OFFICE SYMBOL (If applicable)		9 PROCUREMENT INSTRUMENT IDENTIFICATION NUMBER
8c ADDRESS (City, State and ZIP Code) Washington, DC 20361		10 SOURCE OF FUNDING NUMBERS		
		PROGRAM ELEMENT NO 61153N	PROJECT NO WR02101	TASK NO 532-MP07
		WORK UNIT NO MP07		
11 TITLE (Include Security Classification) A RADAR SEA CLUTTER MODEL FOR ATMOSPHERIC DUCTING CONDITIONS				
12 PERSONAL AUTHOR(S) F. P. Snyder				
13a TYPE OF REPORT Final	13b TIME COVERED FROM <u>Oct 79</u> TO <u>Dec 83</u>		14 DATE OF REPORT (Year, Month, Day) 31 July 1984	15 PAGE COUNT 39
16 SUPPLEMENTARY NOTATION				
17 COSATI CODES		18 SUBJECT TERMS (Continue on reverse if necessary and identify by block number)		
FIELD	GROUP	SUB GROUP	Atmospheric ducting Integrated Refractive Effects Prediction System (IREPS) Sea clutter	
19 ABSTRACT (Continue on reverse if necessary and identify by block number) <p>An updated surface clutter computer model for IREPS is presented, along with some details of the computer implementation. An analysis also is presented which indicates the sensitivity of the model to variations in the environmental parameters required as input to the computer program. Finally, a quantitative validation effort is discussed, though in terms only of data acquired for a single location and a single frequency due to limited assets.</p>				
20 DISTRIBUTION/AVAILABILITY OF ABSTRACT <input checked="" type="checkbox"/> UNCLASSIFIED - UNLIMITED <input type="checkbox"/> SAME AS RPT <input type="checkbox"/> DTIC USERS		21 ABSTRACT SECURITY CLASSIFICATION UNCLASSIFIED		
22a NAME OF RESPONSIBLE INDIVIDUAL F. P. Snyder		22b TELEPHONE (Include Area Code) (619) 225-7400		22c OFFICE SYMBOL Code 544

DD FORM 1473, 84 JAN

83 APR EDITION MAY BE USED UNTIL EXHAUSTED
ALL OTHER EDITIONS ARE OBSOLETEUNCLASSIFIED
SECURITY CLASSIFICATION OF THIS PAGE

CONTENTS

INTRODUCTION 1

THE PROPAGATION AND CLUTTER CROSS SECTION MODELS 3

EFFECTS OF REFRACTIVITY LAYER BOUNDARY PERTURBATIONS 15

MODEL VALIDATION 21

CONCLUSIONS AND RECOMMENDATIONS 26

REFERENCES 39

Accession For	
NTIS GRA&I	<input checked="" type="checkbox"/>
DTIC TAB	<input type="checkbox"/>
Unannounced	<input type="checkbox"/>
Justification	
By _____	
Distribution/	
Availability Codes	
Dist	Avail and/or Special
<i>A-1</i>	



INTRODUCTION

↓
The Integrated Refractive Effects Prediction System (IREPS) should consider sea clutter effects under atmospheric ducting conditions. The IREPS, undergoing research and development at Naval Ocean Systems Center (NOSC), is intended to provide a shipboard environmental data processing and display capability to assess refractive effects of the lower atmosphere for naval EM systems. Although intended to be incorporated eventually as a part of the Tactical Environment Support System (TESS), the IREPS is currently configured as an interim version based on a Hewlett-Packard 9845 desktop calculator. A comprehensive discussion of the IREPS capabilities is presented by Hitney et al. (1981), while a discussion of the IREPS propagation models is presented by Hattan (1982).

Numerous limitations of the IREPS models are listed by Hitney et al. (1981), among which is the fact that surface clutter (land or sea) is not included in the calculation of radar detection ranges. A clutter computer model was developed and was first described by Snyder (1979). Some modifications have subsequently been made to this model and the updated model has been implemented in a computer program in FORTRAN (the language of the original IREPS). This updated model, along with some details of the computer implementation, is discussed in this document. Also presented is an analysis indicating the sensitivity of the model to variations in the environmental parameters required as input to the computer program.

Snyder (1979) concluded that the sea clutter model developed appeared to be adequate, at least qualitatively, for an elevated layer, ground based duct environment, but that some sort of quantitative "validation" effort should be conducted before implementation into IREPS for shipboard use. Because of

manpower and money limitations, an extensive validation effort could not be undertaken. However, using essentially "free" facilities on a "not-to-interfere" basis, validation data were acquired for a single location and a single frequency. That validation effort is also discussed in this document.

THE PROPAGATION AND CLUTTER CROSS SECTION MODELS

Snyder (1979) and Hitney et al. (1981) both point out the occurrence of two types of atmospheric ducts which can be expected to greatly influence sea clutter. One is the evaporation duct, which is formed by the sea surface and the near surface minimum in the refractive index profile, which is in turn determined mainly by the vertical distribution of water vapor resulting from evaporation. The other is a surface based duct formed by an elevated refractive layer.

The propagation environments resulting from the two types of ducts are uniquely different and can be expected to result in two different effects on sea clutter. The evaporation duct would tend to enhance clutter signals over extended areas, whereas the ground based duct formed by an elevated layer would result in clutter signal enhancement only from discrete ranges. Propagation in the two different environments would also best be considered using two different formulations. Vertical dimensions for the evaporation duct are on the order of metres to very few tens of metres and a waveguide mode formulation would be appropriate for this type of duct. Vertical dimensions for the ground based duct formed by an elevated refractive layer are typically on the order of many tens of metres to a few hundred metres and ray-optical formulations would be appropriate here.

The clutter model developed for the IREPS is based on a ray-optical propagation formulation and is therefore most applicable to the surface based duct formed by an elevated refractive layer. The geometrical basis for the propagation formulation is developed in the following way. The propagation environment is assumed to be two dimensional, with the earth represented by a cylinder and propagation in a plane transverse to the cylinder axis. Thus, earth curvature is considered in the direction of propagation but is ignored

transverse to the propagation direction. A classical conformal transformation to Maxwell's equations in cylindrical form is employed, converting the geometry from cylindrical to rectangular (Cartesian). This transformation has been discussed in the context of earth flattening by Richter (1966) and has been widely applied in radiowave and radar propagation problems when earth curvature in the direction of propagation is an important factor. The net effect of the transformation is to change from the cylindrical geometry with refractive index given by n to the rectangular geometry with refractive index given by n multiplied by $\exp(z/a)$, where a is the radius of the earth and, to first order in $1/a$, and z is essentially the altitude above the earth (see Figure 1).

The ray path trajectories are determined from the classical eikonal expression (Jones, 1979)

$$\frac{d}{ds} \left(n \frac{d\vec{r}}{ds} \right) = \nabla n \quad (1)$$

where

s = arc length along a ray path

$n = n(\vec{r})$ = index of refraction at \vec{r}

\vec{r} = position vector ($\hat{x} r_x + \hat{y} r_y + \hat{z} r_z$)

$\hat{x}, \hat{y}, \hat{z}$ = unit vectors

Let

$$t_i = \frac{dr_i}{ds} \quad (i = x, y, z) \quad (2)$$

and use the fact that $(\nabla n)_i = \partial n / \partial r_i$ to rewrite (1) in rectangular form as

$$\frac{d}{ds} (nt_x) = \frac{\partial n}{\partial x}; \quad \frac{dx}{ds} = t_x \quad (3a)$$

$$\frac{d}{ds} (nt_y) = \frac{\partial n}{\partial y}; \quad \frac{dy}{ds} = t_y \quad (3b)$$

$$\frac{d}{ds} (nt_z) = \frac{\partial n}{\partial z}; \quad \frac{dz}{ds} = t_z \quad (3c)$$

Rewrite (3a) as

$$t_x \frac{dn}{ds} + n \frac{dt_x}{ds} = \frac{\partial n}{\partial x} \quad (4)$$

With dn/ds in component form

$$\frac{dn}{ds} = \frac{\partial n}{\partial x} \frac{dx}{ds} + \frac{\partial n}{\partial y} \frac{dy}{ds} + \frac{\partial n}{\partial z} \frac{dz}{ds} = \sum \frac{\partial n}{\partial r_i} t_i$$

equation (4) becomes

$$n \frac{dt_x}{ds} = \frac{\partial n}{\partial x} - t_x \sum \frac{\partial n}{\partial r_i} t_i \quad (5)$$

which can be generalized to all three coordinate directions. Assuming homogeneity in both horizontal directions ($\frac{\partial n}{\partial x} = \frac{\partial n}{\partial y} = 0$) the components of (5) become

$$\frac{dt_x}{ds} = - \frac{t_x t_z}{n} \frac{dn}{dz} \quad (6a)$$

$$\frac{dt_y}{ds} = - \frac{t_y t_z}{n} \frac{dn}{dz} \quad (6b)$$

$$\frac{dt_z}{ds} = \frac{1}{n} \frac{dn}{dz} (1-t_z^2) \quad (6c)$$

If $t_y = 0$ initially, corresponding to a ray having no initial transverse component, then (6b) shows that $t_y = 0$ always. Making this assumption and transforming to the angular variable given by $t_x = \cos\theta$ and $t_z = \sin\theta$ (θ is the ray angle with respect to the horizontal) leads to the expressions

$$\frac{d\theta}{ds} = \frac{1}{n} \frac{dn}{dz} \cos\theta ; \quad \frac{dz}{ds} = \sin\theta \quad (7)$$

The refractive index in (7) is given in terms of the original (cylindrical) refractive index as

$$n = n(z) \exp(z/a) \quad (8)$$

Because the atmospheric refractive index $n(z)$ is only slightly greater than unity, it is convenient to write $n(z) = 1 + \delta n(z)$ where $\delta n \ll 1$. Typically, $\delta n \approx 10^{-4}$ so in order to have a number of more convenient magnitude, the "refractivity" N has been defined to be $N = (n - 1) \times 10^6 = \delta n \times 10^6$.

Expanding the exponential term in (8) and using the modified refractivity, defined as $M = N + 10^6 z/a$, the refractive index can be written as

$$n = 1 + 10^{-6} M \quad (9)$$

Substituting (9) into (7), assuming paraxial rays and writing the angle in milliradians ($\beta = 10^3 \theta$) yields the differential forms

$$d\beta = \frac{1}{\beta} \frac{dM}{dz} dz ; \quad d\beta = 10^{-3} \frac{dM}{dz} dz \quad (10)$$

Integrating the first expression in (10) yields

$$\beta^2 = \beta_0^2 + 2(M - M_0) \quad (11)$$

where β is the angle at the modified refractivity M resulting from initial angle β_0 at M_0 . Integrating the second expression in (10) with the assumption that dM/dz is constant yields

$$x = \frac{\beta - \beta_0}{10^{-3} \left(\frac{dM}{dz} \right)} \quad (12)$$

where the initial condition $x = 0, \beta = \beta_0$ is assumed. The result in (11) is simply a statement of Snell's law in the paraxial approximation and is independent of the way the modified refractivity varies with height. The result in (12), however, is valid only if the modified refractivity varies linearly with height. The modified refractivity profile for the clutter model is thus assumed to be linearly segmented with height.

Some properties of ray paths which are important to the question of sea clutter under ducting conditions are shown in Figure 2. A surface based duct resulting from an elevated refractive layer is shown diagrammatically in Figure 2 as a trilinear M-profile. Assume that a ray source is located at some height, such as position A in the Figure. From (11) a ray will be concave upward within the first linear segment of the profile and concave downward within the second. Further, the magnitude of the slope of any ray trajectory will be the same at all points within the profile with the same M-value, provided of course, that the ray reaches the particular point at all. For example, a ray launched horizontally (labelled [A] in Figure 2) at A will be

continually turned upward until reaching the first change in profile slope and will then begin turning downward. As the ray approaches the height A', where the M-value is the same as at A, the ray trajectory will again approach horizontal and continue turning downward, thus being "reflected" at height A'. The ray trajectory again changes concavity where the M-profile slope changes and is again horizontal at height A, being reflected upward at this height. The ray is thus "ducted" or "trapped" between A and A'.

Consider a ray launched downward at A with such an angle that the continual upward turning will result in a horizontal trajectory just above the surface. Such a ray, labeled [B] in Figure 2, will be trapped between the heights of B and B', as shown in Figure 2. Any ray launched below this ray will reach the lower surface (which is necessary before the ray can contribute to sea clutter) and be reflected according to the usual laws of reflection at a plane interface. There is a launch angle for which a ray will just become horizontal as it approached C' in Figure 2. Such a ray, labeled [C] in Figure 2, will be reflected downward at C' and will thus be trapped between the surface and C'. Any ray launched below this ray (such as ray [D] in Figure 2) will reach the height C' at a non-zero angle and continue upward, escaping through the top of the duct. There is thus a range of downward launch angles for which rays will be both trapped in the duct and reflected off the lower (sea) surface. By symmetry and reciprocity arguments, there is also a family of rays with upward launch angles which will be trapped in the duct as well as be reflected off the lower surface. It is these two families of rays which contribute to sea clutter enhancement under conditions when an elevated refractive layer produces a surface based duct.

In the ray-optical propagation model, a single ray is envisioned as departing the radar, propagating forward, then to be refracted by the atmo-

sphere such as to reach the surface of the sea. Some of the radiated energy is returned (on a reciprocal path) as sea clutter while the bulk of the energy is reflected, propagating forward to be again refracted by the atmosphere to reach the surface of the sea, repeating the procedure. The surface backscatter power returned to the radar (sea clutter) can be conveniently written in terms of the "radar equation" as

$$P_c = P_t \frac{G^2 \lambda^2}{(4\pi)^3 R^4} r^{2(m-1)} \sigma_c \quad (13)$$

where P_c = Clutter power returned

P_t = Power transmitted

G = Antenna power gain

λ = Radar wavelength

R = Radar-to-surface distance along a raypath

r = Sea reflection coefficient

m = Order of the ray-hop

σ_c = Total clutter cross section at range R

In equation (13), the sea reflection coefficient is taken from the work of Ament (1953) as extended by Beard (1961). A similar expression can be written for a target by replacing the term $r^{2(m-1)} \sigma_c$ by the term $F^4 \sigma_t$ (Kerr, 1951) where

F = Pattern - propagation factor at target position

σ_t = Target cross section

The definition of pattern-propagation factors is such that the ranges at which

target detection can occur (without clutter) are given by

$$R < F \cdot R_{fs} \quad (14)$$

where R_{fs} is the range to target detection in free space. If clutter is present, a working definition of target detection is the simultaneous satisfaction of (14) and the requirement that the target power returned exceed the clutter power returned.

$$R < F \cdot R_{fs} \quad \text{AND} \quad P_T > P_C \quad (15)$$

where P_T is the returned target power. In terms of the various cross sections, (15) is equivalent to:

$$F < (\sigma_c / \sigma_t)^{1/4} r^{(m-1)/2} \quad (16)$$

This model is based on a ray-optical propagation model. To accommodate a non-ray optics model, such as the equivalent single mode model used in the IREPS for ducted propagation (Hattan, 1982), note that (16) can be used provided only that a way to determine F as a function of range is available.

The area extensive cross-section of sea return is a function of many variables, including sea state, angle of incidence, aspect angle, radar wavelength and polarization. The clutter cross section model adapted for use with the ray path propagation model was developed at Georgia Institute of Technology and is commonly known as the GIT sea clutter model (Trebits et al., 1978). The model is semi-empirical and calculates the sea clutter cross section normalized per unit area as a product of three factors: sea

direction, windspeed, and multipath. Each factor is a function of the appropriate independent variables. Thus, $\sigma_c = \sigma_o/A$, where σ_o is the normalized cross section (see Figure 3) and A is the pulse length limited area given by

$$A = \frac{c\tau}{2} R \theta$$

where

c = speed of light

τ = pulse length

R = range

θ = horizontal beam width

The model assumes a "fully arisen" sea for which wave height and wind speed are coupled under the assumption of equilibrium conditions. Both the wind/sea direction dependence and the wind speed dependence of the cross section model are empirically derived. The multipath portion of the model has a theoretical basis.

The sea clutter cross section per unit area is shown in Figure 3 for two radar frequencies (C-Band and L-Band) at several wind speeds. Both upwind and downwind values are shown for a 15-knot wind speed. Some properties of the sea clutter cross section per unit area are to be especially noted. For high wind speeds, the sea clutter cross section for the C-Band increases very rapidly at very small grazing angles, reaching a nearly constant value between five and ten milliradians. This property is also exhibited at L-Band, although not so dramatically. For both bands, there is a large sensitivity to variations in wind speeds for moderate speeds. For example, there is as much as a 20 dB change in cross section between 10-knot and 15-knot winds. There is a much decreased sensitivity to changes in wind speed at higher wind

speeds, although the clutter cross sections are much larger for higher wind speeds. Note also that the directional dependence of clutter cross section is insensitive to the actual windspeed and grazing angle, although there is some sensitivity to the radar band, with the larger directional dependence at higher frequencies.

The computer implementation of the model was effected in the following way. Reference modified refractivities are computed corresponding to the levels in Figure 2 at C' (denoted by M_u), at B (denoted by M_d) and at A (denoted by M_t). The occurrence of a surface based duct is determined if $M_u < M_d$ and the radar is in the duct if $M_t > M_u$. If these are satisfied, the launch angle (β_d) for the surface grazing ray ([B] in Figure 2) and the launch angle (β_u) for the ray just grazing at C' ([C] in Figure 2) are computed. The rays that are trapped and also contribute to sea clutter are found within the limits $|\beta_u - \beta_d|$ both above and below the horizontal. This fan of rays is divided into 30 equally spaced rays (β_j), and for each ray the following are computed:

β_{sj} = grazing angle at sea surface for j-ray.

ρ_{uj} = surface distance for the upward launched j-ray to be "reflected" and return to the sea surface.

ρ_{dj} = surface distance for the downward launched j-ray to reach the sea surface.

$\Delta\rho_j$ = skip distance for the j-ray = $\rho_{uj} + \rho_{dj}$

σ_{cj} = sea clutter cross section for j-ray (normalized per unit area)

r_j = sea surface reflection coefficient for j-ray

The β_{sj} are computed using (11) and the ρ 's are computed by iterative application of (12) for each ray.

The propagation path is divided into 100 range bins of 2 km each. A recursive procedure is then employed to determine the contribution to the total clutter power due to each successive hop for both the upward launched and downward launched ray sets. Values within any given range bin are determined by linear interpolation between two j-rays if a single ray does not "land" within the bin. The 100 elements of the range bin array are finally modified to include a preset but arbitrary target cross section and appropriate roots are taken to provide the right hand side of (16).

The operational implications of the combined ray path propagation model and normalized clutter cross section model can be qualitatively inferred from the considerations of the individual aspects already discussed. It can be expected, for example, that at high wind speeds, even moderately strong surface based ducts will result in enhanced clutter effects. The clutter ring "splitting," mentioned previously (Snyder, 1979) in regards to the USS ENTERPRISE demonstrations of the IREPS, can be inferred from the existence of two sets of influential rays (the initially upgoing and downgoing launched sets). The existence of clutter rings in only a limited angular sector might be inferred by the directional dependence of the clutter cross section, but horizontal inhomogeneity in the environment would seem a more likely cause.

The clutter effects model was coded and implemented into a special FORTRAN version of the IREPS. Typical results are presented in the "coverage diagrams" of Figures 4-6. A hypothetical C-Band radar with 100-nmi free space

detection range against a reference target of two square metres cross section is assumed located at 140 feet height. As a reference, the coverage diagram for a nonducted (standard) atmosphere with a 10-knot wind is shown in Figure 4. Recall that the darkened area of the diagram represents the range/height conditions where the radar would detect the target.

A coverage diagram for the same wind conditions, but for a surface based duct, is shown in Figure 5. The elevated refractive layer causing this duct is located at about 300 metres and is 40 metres thick. The M-unit deficit between the surface and the layer minimum is 40 M-units. Notice the enhanced coverage for low altitudes to longer ranges. For this case, any clutter effects are just barely observed. A coverage diagram for the same refractivity profile but for a 15-knot wind is shown in Figure 6. For this case, the predicted effects of clutter are quite dramatic. Within the darkened areas of the diagram, target detection would be expected. However, within the areas no longer darkened compared to Figure 5, the target would be undetectable compared to clutter. The presence of clutter in this case would appear on a PPI type display as bright rings, masking the target.

EFFECTS OF REFRACTIVE LAYER BOUNDARY PERTURBATIONS

An important property of the clutter model is the ability to predict characteristics of clutter rings. A crucial factor in this ability is the properties of the vertical modified refractivity profile. Variations in the profile boundaries can be expected to produce variations in the clutter ring characteristics. For this reason, effects of both bulk and localized variations in profile boundaries have been examined.

Typical sensitivities of computed clutter ring locations to bulk variations in boundary heights for elevated layers are shown in Figure 7. The figure shows the location of the first and second clutter rings for a trilinear profile as a function of layer thickness and parametric in layer height. In this example, variation in layer thickness results from changes in the slope of the modified refractivity within the elevated layer with no change in the height of the bottom of the layer, the slope of the lowest region of the profile (called $\Delta M/\Delta h_0$ in Figure 7), or the net M-deficit (called ΔM in Figure 7). The geometrical change in the profile is shown in the figure insert. The change in clutter ring location per metre change in layer thickness is approximately 0.2 nmi for the first ring and 0.3 nmi for the second. These results depend only very slightly on the layer height or thickness.

An alternate variation in layer thickness, resulting from raising the height of the layer while maintaining a fixed gradient both within and below the layer as well as a fixed M-deficit was also considered. For this situation, the change in clutter ring location per metre change in layer height is approximately 0.1 nmi for the first ring and 0.2 nmi for the second. Just as for the previous case, these results are insensitive to the specific layer height or thickness.

From these and other similar results, it is concluded that bulk changes in refractive layer height or thickness on the order of a few metres will only slightly change the apparent clutter ring location on a typical PPI display. Bulk changes of such an order might be expected over short periods, perhaps on the order of a few tens of minutes. Over periods of a few hours or longer, bulk changes on the order of tens of metres in refractive layer height or thickness may be expected. For such longer periods, changes of a few miles in clutter ring location might be expected.

The actual occurrence of clutter rings is a more sensitive function of refractive layer configuration than is the variation in location. Changes in layer height or thickness are usually accompanied by changes in M-deficit. This results in changes in the grazing angle and consequently in the clutter return signal. Bulk changes in height or thickness of elevated refractive layers are thus expected to lead to clutter rings which fade "in-and-out" on a typical PPI display while remaining nearly fixed in location.

The effects of bulk changes in the boundaries of the refractive layer formed by a surface evaporation layer have also been considered. The evaporation layer was modelled simply with a single negative M gradient at the surface, changing to a positive gradient at height h_0 as shown in the insert to Figure 3. Although ray optical methods are generally inadequate for complete quantitative analysis of propagation in the evaporative duct, the method is believed adequate to describe qualitative and quantitative trends resulting from modifications in evaporative duct parameters. Two types of changes were considered, one with constant layer strength (height) and variable M-deficit and the other with fixed M-deficit and variable layer strength. Typical results for variable M-deficit are shown in Figure 8. In the figure, an evaporation layer with minimum M-value at ten metres and vari-

able M-deficit is superimposed on a modified refractivity profile with a 50-metre-thick refractive layer at a height of 300 metres. The original profile (without evaporation layer) produces a ground based duct with a 30 M-unit deficit. A diagrammatic picture of the modified refractivity profile is included in Figure 8.

Figure 8 shows that the location of clutter rings is very insensitive to the change in M-deficit. In fact, for the range of M-deficits considered, the change in clutter ring location is less than 0.1 nmi. However, the clutter return cross section is seen to be a sensitive function of the M-deficit, increasing in excess of 3 dB for the range in M-deficit shown. Thus, for this type of bulk profile modification, clutter rings would exhibit exceptional spatial stability with variable intensity.

The alternate variation in evaporation layer, characterized by a fixed value to M-deficit and variable layer height (h_0 of Figure 8), showed a significant sensitivity of computed ring location to layer height (or layer strength). Because the M-deficit remained constant, and therefore also the grazing angle, the clutter model predicts this type of profile modification produces no change in the clutter return signal.

The variations in clutter ring characteristics due to modelled variations of an evaporation layer thus differ both qualitatively and quantitatively from the results for variations of an elevated layer. In particular, clutter ring location is reasonably stable for bulk variations in elevated layers, but highly variable for bulk variations in evaporation layer. Furthermore, much larger changes in ring intensity would be expected for evaporation layer variations.

Localized variations in layer boundaries were modelled in terms of spatially periodic fluctuations of layer boundaries. Two forms of perturbations

were considered, one a sinusoidal variation in evaporation layer strength (height) and the other an exponentially damped sinusoidal variation in refractivity at the boundary of an elevated refractive layer. Numerical integration of the three-dimensional ray equation was used. The eikonal equation in rectangular component form (see equation 5) was employed with the assumption that $\partial n / \partial y = 0$ so that n had only a two-dimensional variation (z -vertically; x -in the horizontal propagation direction). Also, an arbitrary initial ray direction and position were permitted. The coupled equations (5) were solved with a fourth-order Runge-Kutta routine using a comparison with second-order to control step size adjustment.

The use of the raytrace formulation of (5) requires an analytic expression for the refractive index. In order to approximate the trilinear profiles used previously, the procedure of Booker (1977) was adopted. The steps in this procedure are depicted in Figure 9. A prototype modified refractivity profile composed of linear segments with slopes A_j is assumed. The transition from one slope to another is modelled by the analytic expression (A). By an appropriate selection of the "scale height" (H), the slope rapidly approaches A_1 for $z < z_2$ and A_2 for $z > z_2$. A generalization to a multislope profile is given by expression (B). The final analytic form of the modified refractivity is found by integrating expression (B) and is given by expression (C). A sample of the use of the algorithm to generate profiles is shown in Figure 10. In the figure, the prototype profile is trilinear and the results for two scale heights ($H = 20$ km and 5 km) are included. A scale height of 5 km was used for the modified refractivity profiles.

Numerous raytraces were computed using a variety of modified refractivity profiles. Sample raytraces showing the effects of the sinusoidal perturbations are given in Figure 11. The effects of a periodic elevated layer are

shown in Figure 11a. The unperturbed refractivity profile is the same as in Figure 10. The sinusoidally perturbed modified refractivity is given by

$$M(x,z) = M_0(z) [1 + A \exp((z_0 - z)^2/\lambda_z^2) \sin(2\pi x/\lambda_x)]$$

where $M_0(z)$ is the unperturbed refractivity, $A = 10$, $z_0 = 300$ m, $\lambda_z = 5$ m, and $\lambda_x = 10$ km. The significant point of Figure 11a is the fact that the range to reflection or turning points of the lowest order hops is only slightly affected by the perturbation. What is significantly affected is whether or not a ray reaches the surface. These characteristics, which were found to be typical in general for the elevated layer refractivity perturbations considered, would result in clutter rings "fading in-and-out" with only slight fluctuations in location.

The effects of a periodic perturbation to the evaporation layer are shown in Figure 11b. The unperturbed profile is the same as for Figure 11a but with a model evaporation layer such as shown in Figure 8 appended. In this case, the layer strength (height, h_0) is 20 m and the additional M-deficit is 20 M-units. The sinusoidally perturbed layer height is given by

$$h(x) = h_0 + A \sin(2\pi x/\lambda_x)$$

where h_0 is the unperturbed height (20 m), $A = 2$ m, $\lambda_x = 2$ km. Most of the rays of Figure 11b are only slightly modified by the layer perturbation. However, a significant effect is demonstrated on one ray, where it is seen that the perturbation causes trapping within the evaporation layer. This trapping, which would result in an increased clutter return from an extended area, is very sensitive to the properties of the evaporation layer.

Just as for the bulk profile modifications, the variations in clutter ring characteristics differ for evaporation layer fluctuations as compared to elevated layer fluctuations. Clutter ring locations are very variable for evaporation layer fluctuations but quite stable for elevated layer fluctuations. These characteristics are the same as for bulk variations in refractive layers. Thus, clutter signal characteristics on a typical PPI display might indicate the type of refractive layer fluctuations, whether evaporation layer or elevated layer. The characteristics could provide only limited information about the extent of the fluctuations, whether localized or widespread.

MODEL VALIDATION

The sea clutter model presented here employs a union of classical one-dimensional ray-optics propagation with a semiempirical normalized sea clutter cross section model not originally intended for application in this manner. The model predictions are in agreement with what limited data could be found for sea clutter return under ducting conditions. These data, in general, concern the geometrical aspects and not the amplitude aspects of the clutter signals. Therefore, it is recognized that some sort of quantitative "validation" effort should be conducted before implementation into the IREPS for shipboard use.

Because of manpower and money limitations, an extensive validation effort has not been possible. However, a NOSC tenant activity, the Integrated Combat Systems Test Facility (ICSTF), agreed to permit use of one of the test radars on a limited, "not-to-interfere" basis for the acquisition of model validation data. The radar employed was an operational fleet type C-band radar (an SPS-10) permanently shore base mounted overlooking the SOCAL OPAREA (Southern California Operating Area).

Modification of the SPS-10 necessary to permit sampling of return signals is diagrammatically depicted in Figure 12. Data are recorded on cassette tape using a microprocessor controlled Data Acquisition System (DACQ). The microprocessor permits sampling with a two-minute averaging of as many as 100 range bins (spaced from 0.25 nmi to 1.22 nmi) at each of 18 or fewer directions with a variable angular spacing of from approximately three degrees to eleven degrees. The fundamental timing for the DACQ is derived from the SPS-10 trigger. The target return signal is sampled at the IF-Amplifier, prior to detector circuits, and passed through a log-detector before averaging and recording. Provisions for display of data sample point locations on a PPI

display unit, along with conventional PPI target display, are included.

Some preliminary data were obtained in order to check out the operation of the DACQ, particularly the timing operations. One set of data was obtained in January 1980 during a period of moderately high winds (15 kts average with gusts to 20 kts). Sea clutter return signals for this case are shown in Figure 13. Shown in the Figure are data for two different two-minute averages, the upper corresponding to 18 radials, spaced 6.3° apart for a total of 107° with range cells every 0.97 nmi, and the lower corresponding to 18 radials spaced 3.5° apart for a total of 60° with range cells every 0.32 nmi. The two sets of curves have nearly identical range dependence, indicating proper operation of the DACQ timing. The large signal centered around 18.5 nmi in the upper figure is from the Coronado Islands, south of San Diego.

A second set of data was obtained in April during a period of ducted propagation but very low wind speeds. As before, two different range bin and angular separations were employed. A plot of the radar return signal is shown in Figure 14. The keypoint in the figure is the strong signal from about 55 nmi to 65 nmi, which is the correct range for the Santa Catalina and San Clemente Islands. Figure 15 shows an additional verification of this. The figure is a map of a portion of the SOCAL OPAREA. The straight lines from San Diego are the data bearings, according to the DACQ timing, and the darkened areas on the lines represent the radar return signals. The positions of San Clemente and Santa Catalina Islands are clearly indicated in the signal return. The return on the central path corresponds to the location of the very small Santa Barbara Island, which is not shown on the map. The "Xs" indicate positions of ships reporting sea state information at any time during the three hours preceding or following the data recording. The first numeral represents the sea wave height and the second represents the swell. Note that

the waves were not sufficient to produce clutter signals.

Based on these and other similar data, it was concluded that the DACQ unit operated properly. The model validation requires not just the occurrence of ducted propagation, which happens frequently in the SOCAL area, but also the occurrence of a sea state sufficient to provide significant clutter return. The occurrence of both together is very rare. The procedure followed was to anticipate the occurrence of ducted propagation, such as through analysis of local weather patterns, and to operate the DACQ whenever such propagation conditions were available, provided the use of the SPS-10 would not interfere with dedicated ICSTF activities. The limitation to normal working hours, which automatically eliminated weekend recording periods, the weekly service schedule, which eliminated one day a week, and the "normal" radar usage, which averaged about two days a week, left little time for a "not-to-interfere" usage. Nevertheless, several hours of return signals were recorded during ducted propagation conditions. Unfortunately, only one set of data, obtained in September 1980, had a sea state sufficient to result in sea clutter return.

The propagation conditions occurring during this time are shown in Figure 16. Figure 16a shows refractivity conditions obtained in the San Diego area on September 30, 1980 at 1200 Z and 2155 Z. The refractivity layer formed at an altitude of approximately 300 metres in the near shore region and, as can be seen, was very stable for at least a twelve-hour period with an M-deficit of approximately 30 M-units. Figure 16b shows refractivity profiles obtained at Point Mugu, north of San Diego, for the same time period. In this case the refractivity layer, also formed around 300 metres, was more variable, but nevertheless persisted over the full twelve-hour time period. The M-deficit for Point Mugu varied from a value in excess of 40 M-units to as small as 15

M-units for this time period. The wind speed at surface level reported by ships in the area varied from slight to moderate. Visual observations at NOSC indicated moderate white cap formation.

A normalized sea clutter power versus range was calculated using the models previously discussed. An example of these results is shown in Figure 17 for the refractivity profiles obtained at NOSC at 2155 Z. The key point to notice is the large increase in clutter power at a range of approximately 40 nmi and the second increase at a range of approximately 90 nmi. The second increase, however, only reaches a level approximately 15 dB below the 40-nmi results. The clutter power results presented in Figure 17 are quite typical of the results obtained for the profiles persisting throughout the time period presented in Figure 16.

Radar backscatter signals averaged over a two-minute period were recorded at approximately 30-minute intervals during the same time period of Figure 16. Results obtained for a short period between 2000 Z and 2300 Z are shown in Figure 18. The presentation in Figure 18 shows essentially a tracing of what would be displayed on a PPI radar scope, superimposed on a map of the geographic area. Note the darkened outline around San Clemente Island. This represents the large signals returned from the island. The signals returned from very large distances, such as from Santa Barbara Island, which is approximately 100 nmi from the radar, indicates the generally extensive persistence of the surface based ducting region which occurred during this time period. Because only limited angular sectors could be examined at any given time with the data acquisition system, not all angular sectors are included in this time period. For those sectors which are included there is generally a significant signal return from the 30- to 50-nmi range, which is consistent with the model predictions. The relative signal strengths from the

various sectors differed considerably, by as much as 15 to 20 dB. Because each sector was sampled at different times, these variations are possibly caused by spatial and temporal variations in refractivity and wind speed.

A major requirement in the validation of the clutter model is the availability of the clutter return absolute amplitude. The measurement of appropriate voltages along the radar input circuits while using a calibrated input at the antenna was not possible due to radar use limitations. The calibration procedure used employed a small calibrated target (of known cross section) being towed radially away from the radar site. The target was mounted on a 2.5-metre mast, made of plastic sewer pipe, and the mast was mounted on a small rubber raft using all nonconducting materials. The raft and mast arrangement was then towed at slow speed (5 kts) using an 800-foot tow line. In the intervening time between the acquisition of the September 30, 1980 data and the calibration data, numerous modifications were made in the SPS-10 radar by ICSTF technicians. Included were changes in the antenna feeds as well as numerous electronic components within the radar proper. Because of this, absolute calibration for the September 1980 data is unavailable.

CONCLUSIONS AND RECOMMENDATIONS

A radar sea clutter model based on a ray-optics propagation formulation combined with a semi-empirical normalized sea clutter radar cross-section has been presented. A preliminary form of the model was coded in FORTRAN for incorporation into the IREPS. The model was exercised for typical propagation conditions and found to be in agreement with what limited observation data are available. A single frequency, single location validation effort was conducted. Model and observed results were in agreement, although absolute amplitude data were not obtained.

A multifrequency and multilocation validation effort should be conducted using dedicated equipments. The locations should be selected to optimize the occurrence of ducted propagation and significant sea clutter return. Incorporation of clutter models into IREPS should be done only after a successful validation effort.

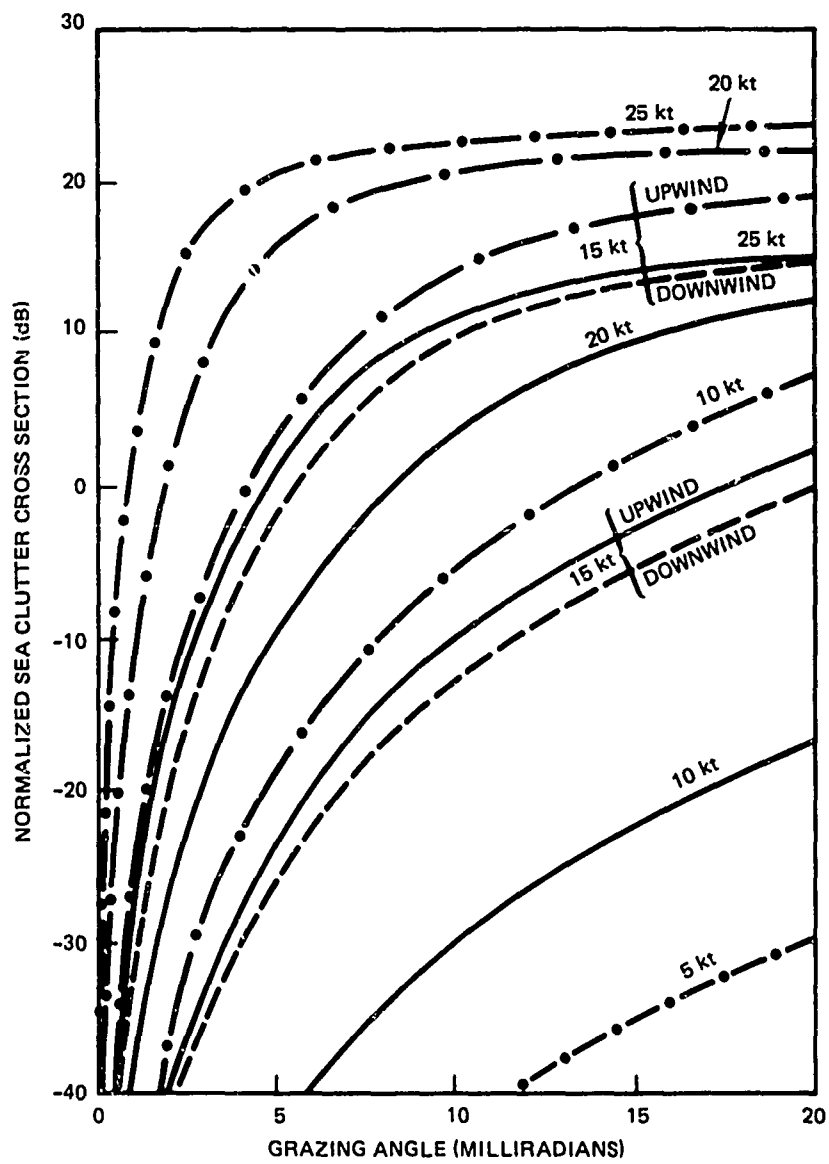


Figure 3. Normalized sea clutter cross-section (relative dB) vs grazing angle (-1300 MHz; - · -5600 MHz).

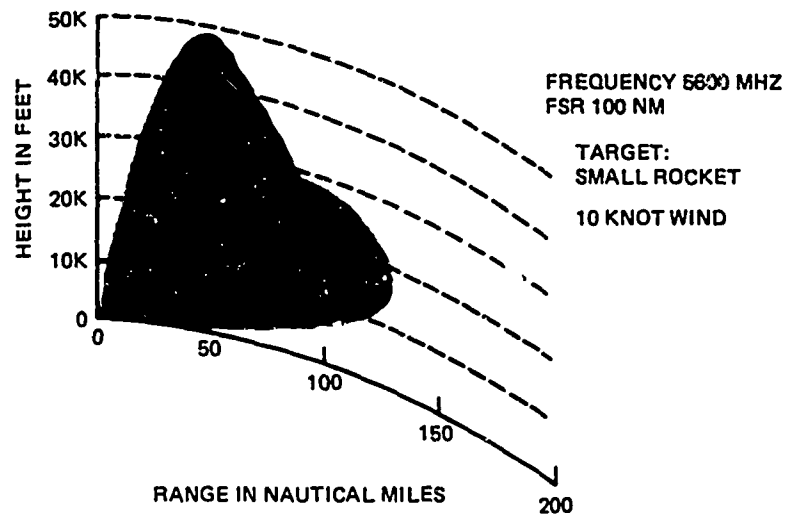


Figure 4. Coverage diagram for hypothetical C-band radar – standard (non ducted) atmosphere.

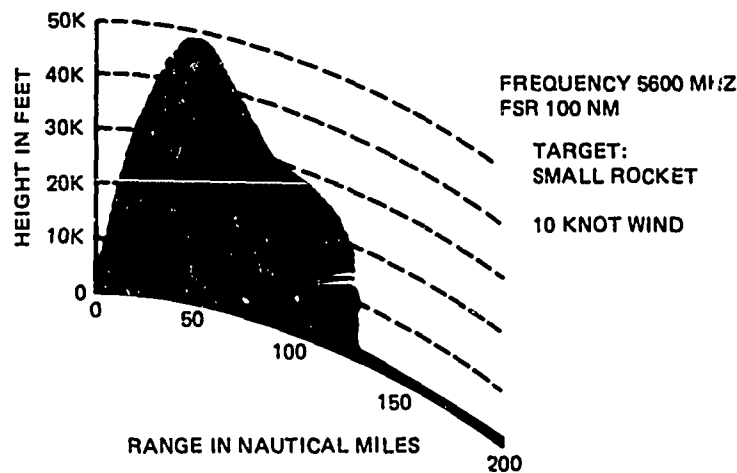


Figure 5. Coverage diagram for hypothetical C-band radar – surface based duct. Duct height - 300 metres; refractive layer thickness - 30 metres.

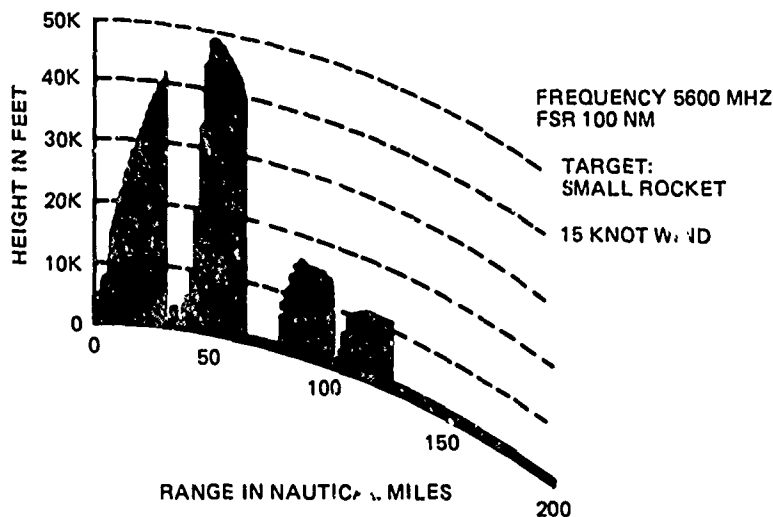


Figure 6. Coverage diagram for hypothetical C-band radar – surface based duct. Duct height - 300 metres; refractive layer thickness - 30 metres.

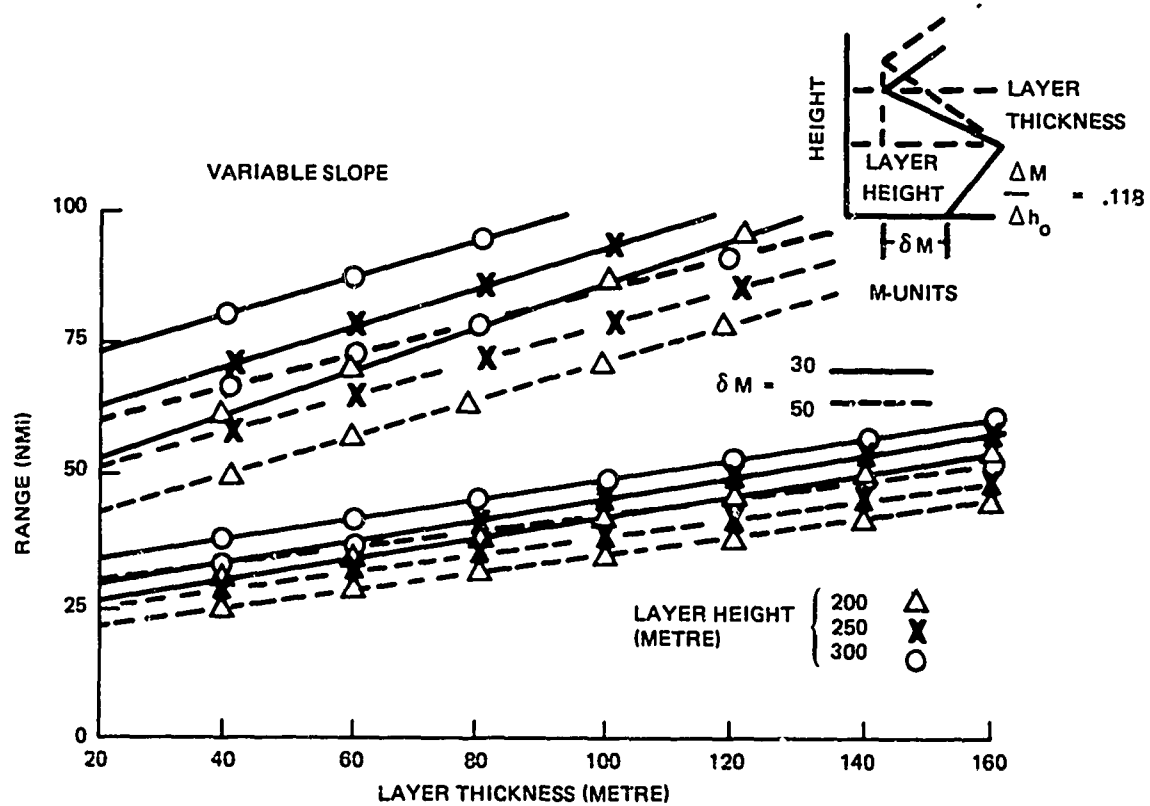


Figure 7. Range to clutter rings vs layer thickness for various layer heights and M-deficits.

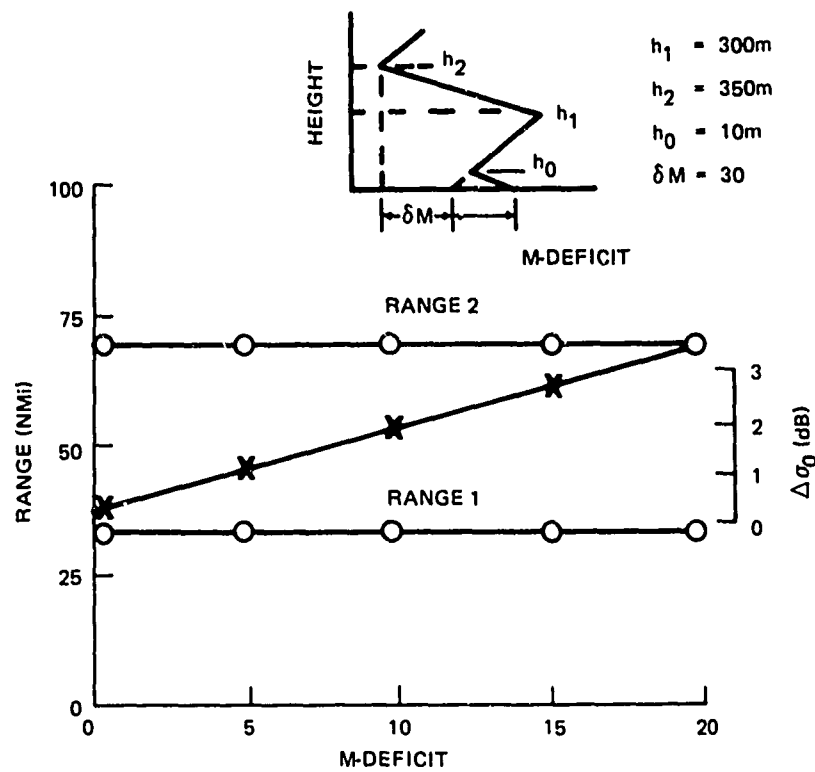
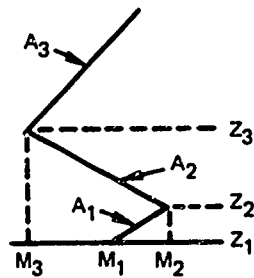


Figure 8. Change in range to clutter rings and clutter return cross-section ($\Delta \sigma_0$) vs change in M-deficit for evaporation layer.



PROTOTYPE

$$\frac{dM}{dZ} = A_1 \quad Z_1 < Z < Z_2$$

$$\frac{dM}{dZ} = A_2 \quad Z_2 < Z < Z_3$$

$$\frac{dM}{dZ} = A_3 \quad Z_3 < Z$$

(A) $\frac{dM}{dZ} = A_1 + \frac{A_2 - A_1}{1 + e^{-(Z - Z_2)/H}}$ \rightarrow $A_1 \quad Z < Z_2$
 $A_2 \quad Z > Z_2$

(B) $\frac{dM}{dZ} = A_1 + \sum_{j=2}^N \frac{A_j - A_{j-1}}{1 + e^{-(Z - Z_j)/H_j}}$ $A_j; Z_j; \text{KNOWN}$
 $H_j; \text{SELECTED}$

(C) $M = M(Z_1) + (Z - Z_1)A_1 + \sum_{j=2}^N (A_j - A_{j-1}) H_{j-1} \ln \left(\frac{1 + e^{(Z - Z_j)/H_{j-1}}}{1 + e^{(Z_1 - Z_j)/H_{j-1}}} \right)$

Figure 9. Development of analytic profile for ray trace.

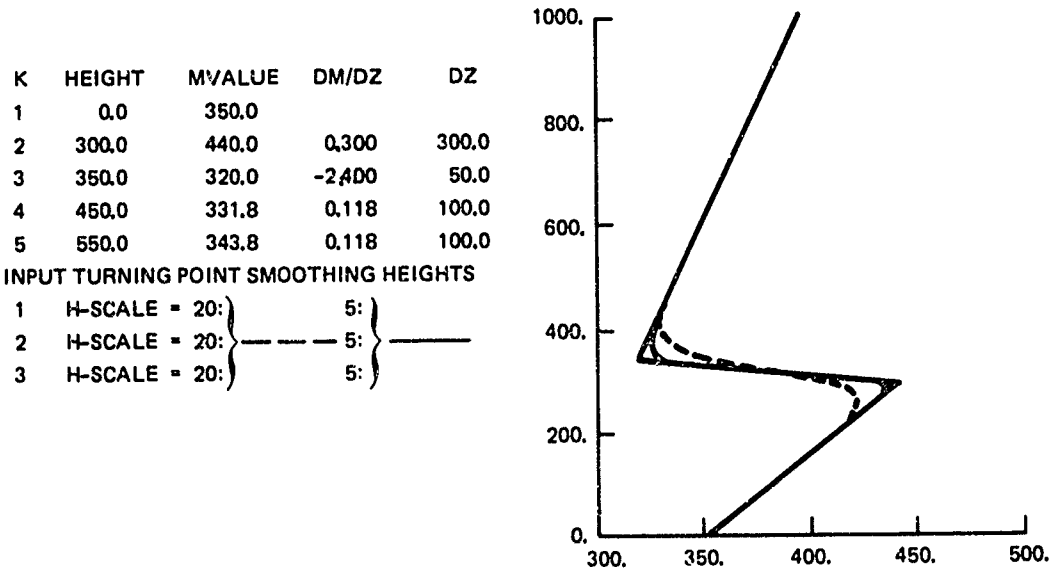


Figure 10. Sample of analytic profile generation.

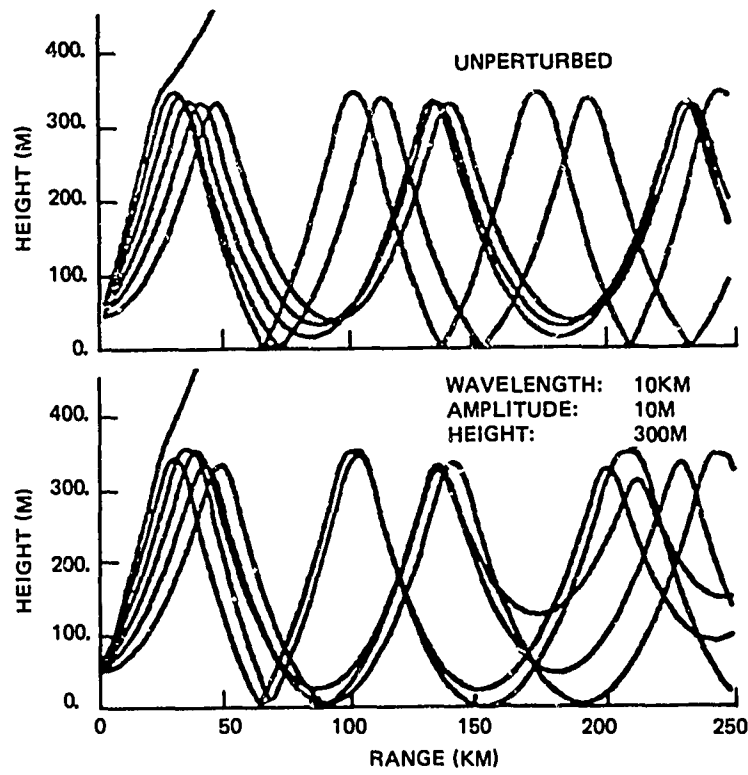


Figure 11a. Sample effect of periodic elevated layer.

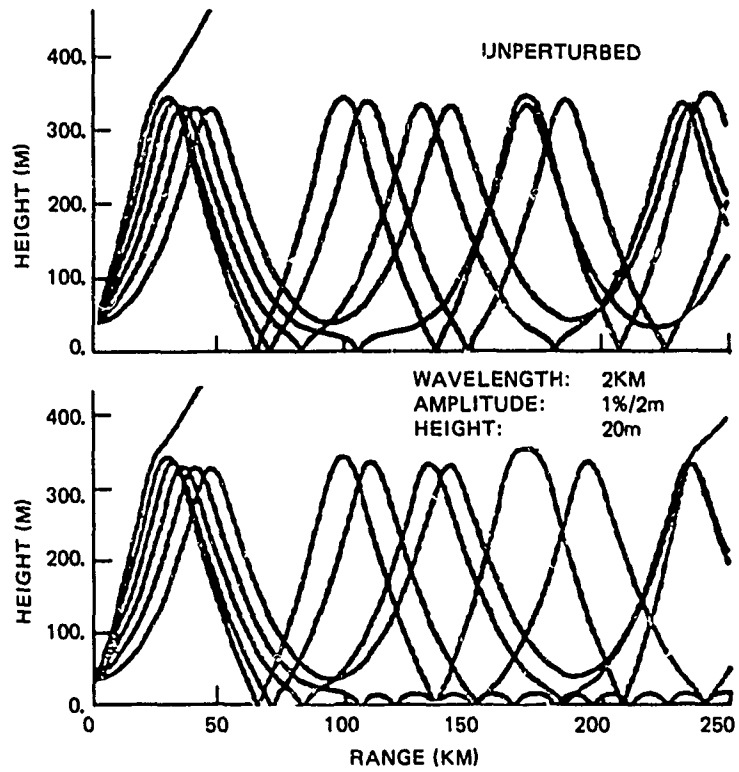
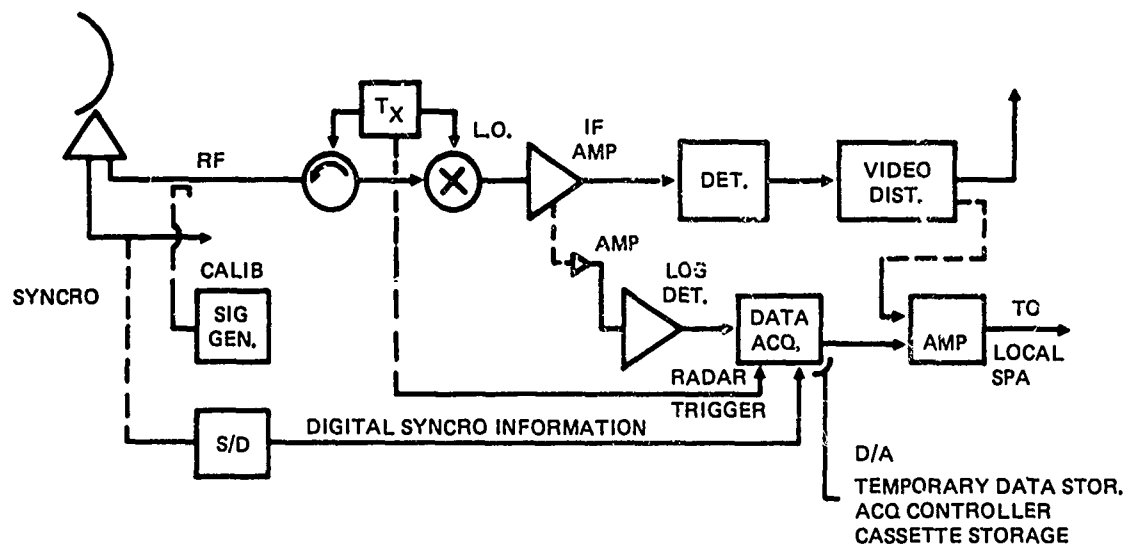
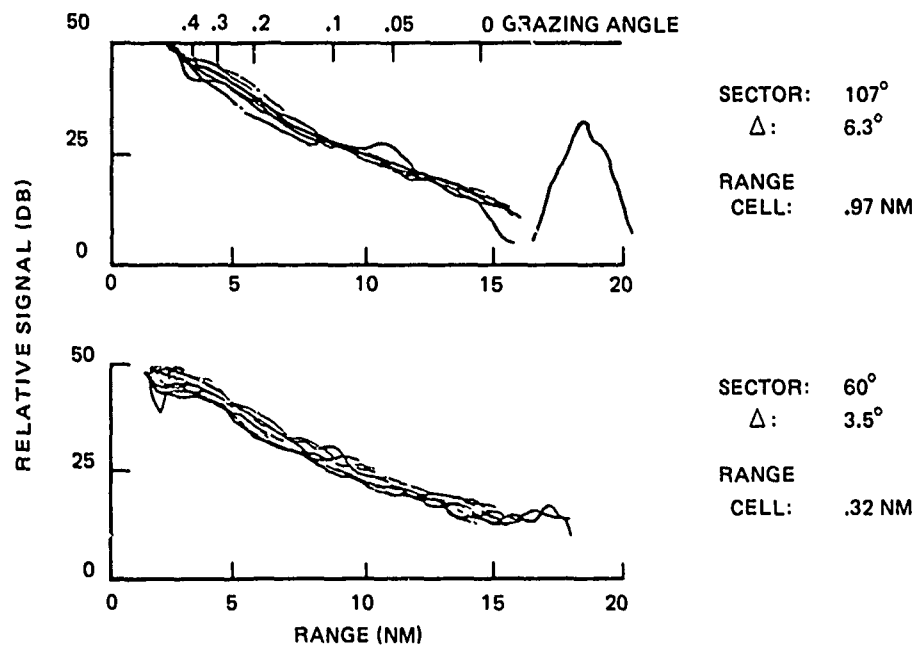


Figure 11b. Sample effect of periodic evaporation layer.



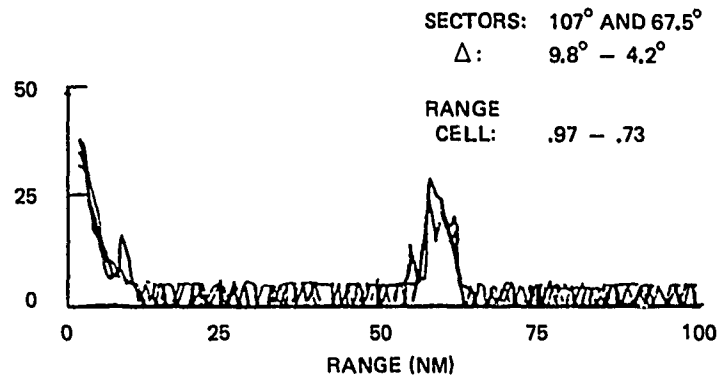
FREQ: 5600 MHZ (C-BAND)
 PULSE RATE: 325 ppi
 MAX RANGE: 240 KM

Figure 12. Modifications to SPS-10 radar.



DATE: 1/18/80
 WIND SPEED: 15 KTS - GUSTS TO 20 KTS

Figure 13. Sample signals with nonducted propagation.



DATE: 4/16/80
 WIND SPEED: LESS THAN 5 KTS

Figure 14. Sample signals with ducted propagation.

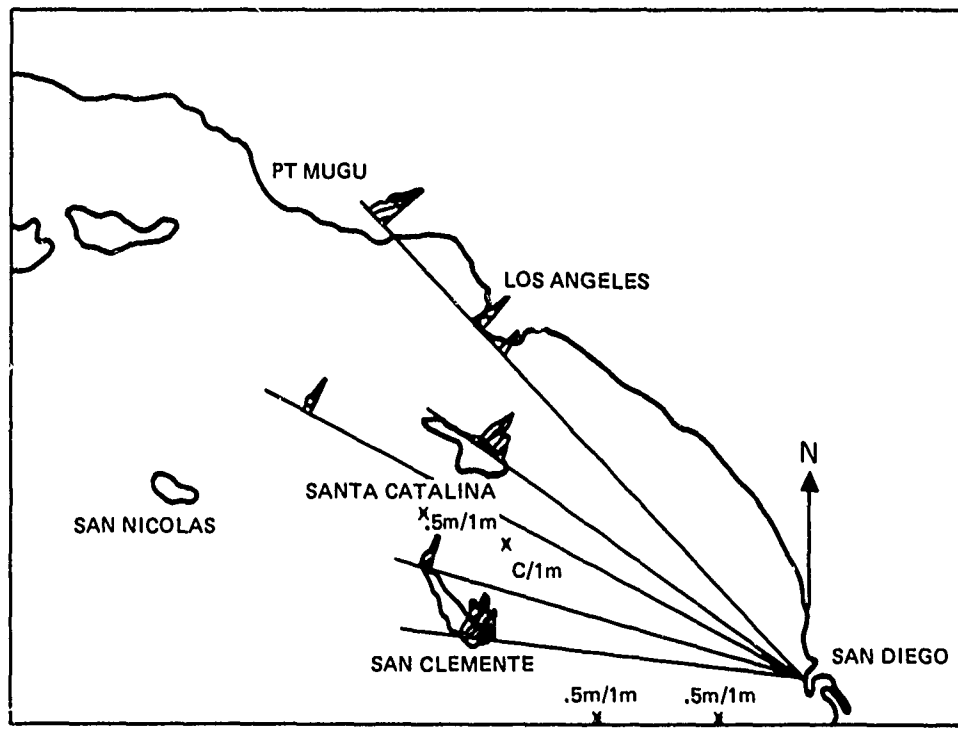


Figure 15. Map of SOCAL OP-AREA depicting radar return.

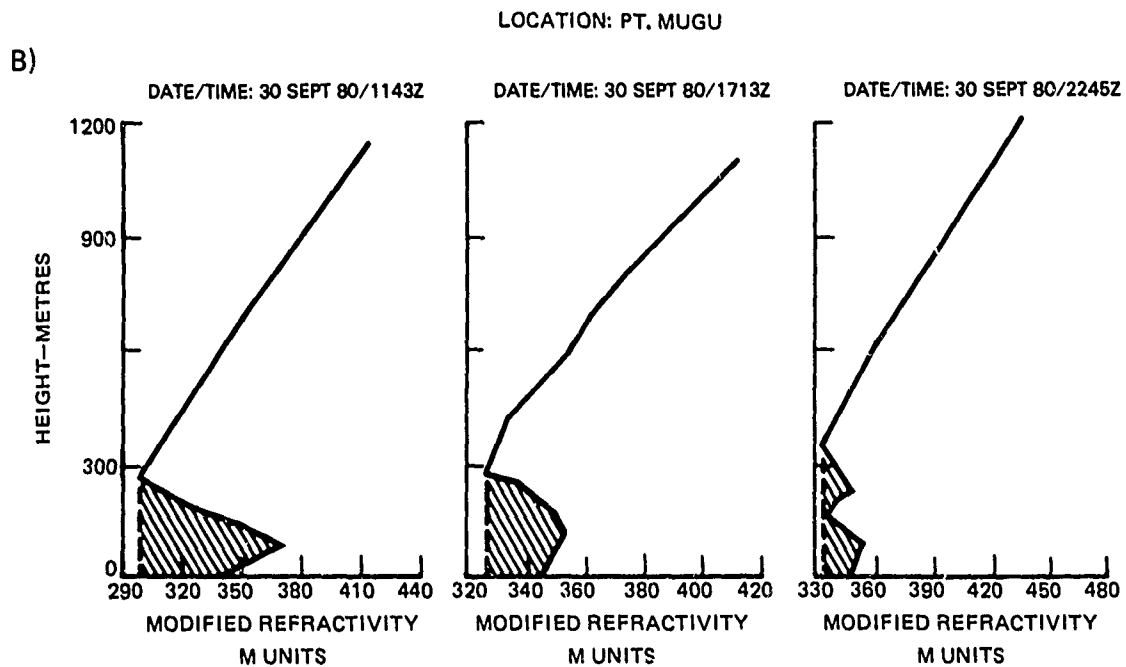
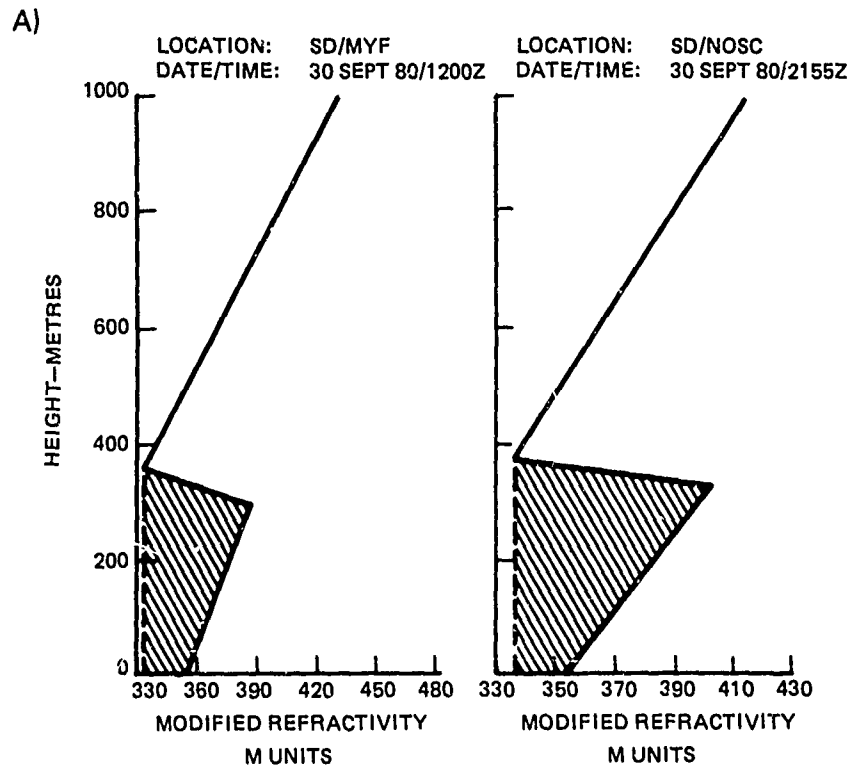


Figure 16. Modified refractivity profiles
 A) San Diego, California
 B) Point Mugu, California.

LOCATION: SD/NOSC
DATE/TIME: 30 SEPT 80/2155Z

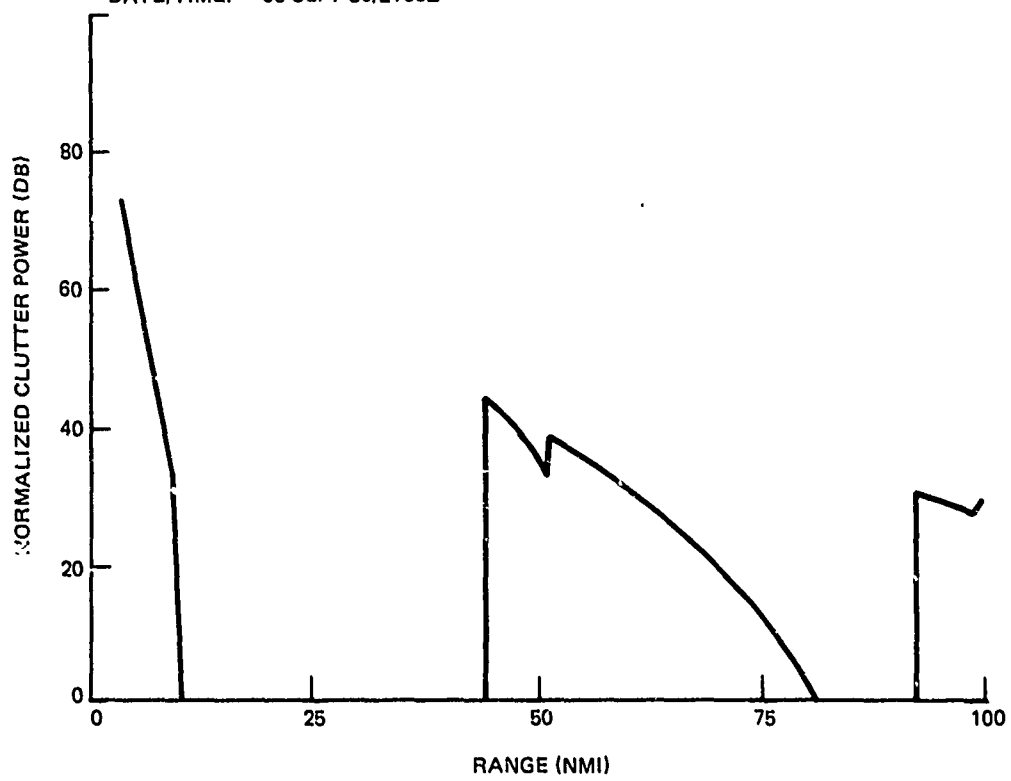


Figure 17. Normalized clutter power (computed).

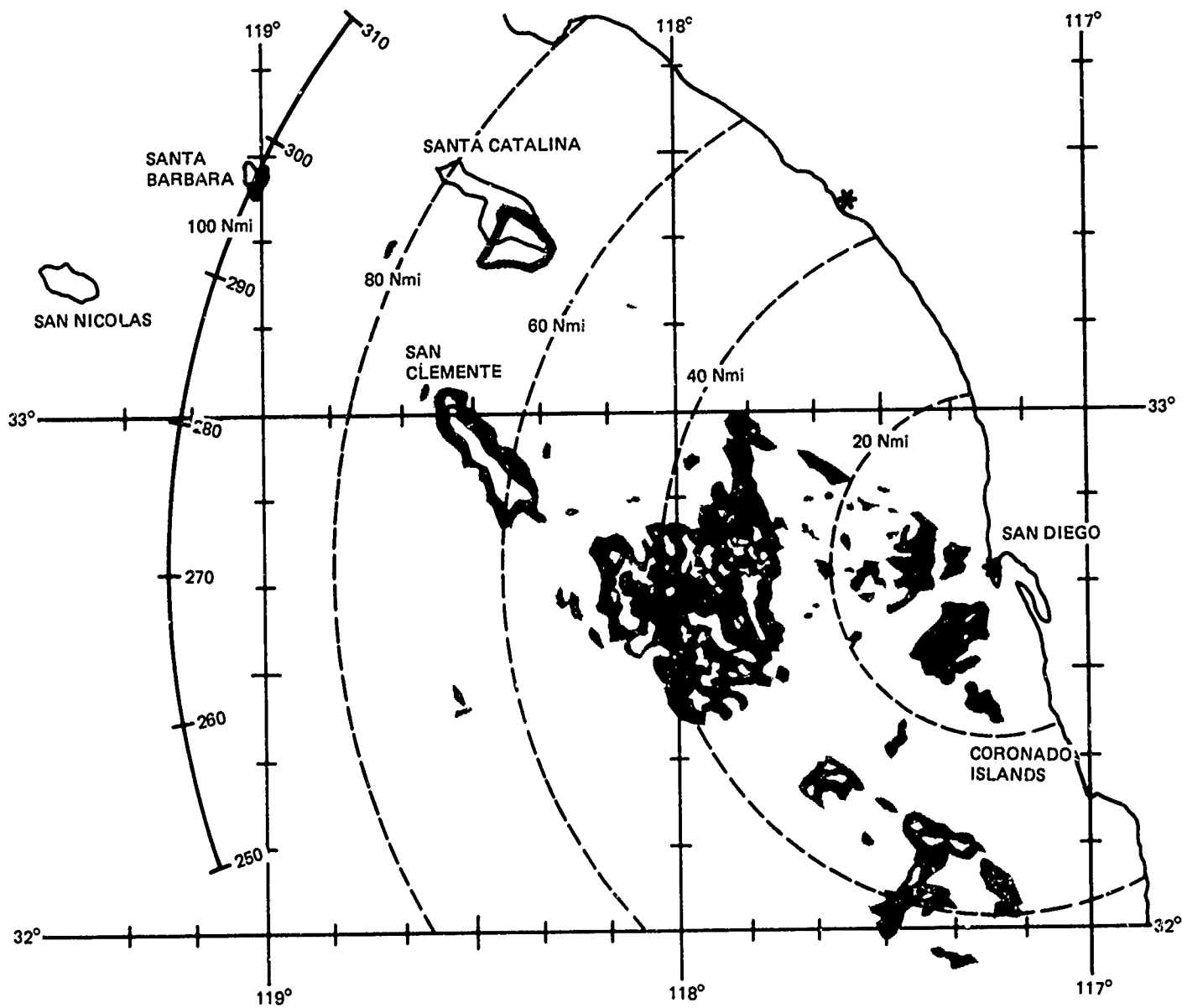


Figure 18. Measured radar signals superposed on regional map to depict a PPI type display.

REFERENCES

- Ament, W. S., "Toward a theory of reflection by a rough surface," Proc. IRE., 41, No. 1, 142-146, January 1953
- Beard, C. I., "Coherent and incoherent scattering of microwaves from the ocean," IRE Trans., Vol. AP-9, September 1961.
- Booker, H. G., "Fitting of multi-region ionospheric profiles of electron density by a single analytic function of height," Jour. Atmos. Terr. Phys., Vol. 39, pp 619-623, 1977.
- Hattan, C. P., "Propagation models for IREPS revision 2.0," NOSC TR 77: April 1982.
- Hitney, H. V., R. A. Paulus, C. P. Hattan, K. D. Anderson, G. E. Lindem, "IREPS revision 2.0 user's manual," NOSC TD 481, September 1981.
- Jones, D. S., Methods in Electromagnetic Wave Propagation, Clarendon Press, Oxford, 1979.
- Kerr, D. E. (ed.), "Propagation of short radio waves," MIT Radiation Laboratory Series, Vol. 13, McGraw-Hill, New York, 1951.
- Richter, J. H., "Application of conformal mapping to earth-flattening procedures in radio propagation problems," Radio Science, Vol. 1, No. 12, December 1966, pp. 1435-1438.
- Snyder, F. P., "Radar clutter under atmospheric ducting conditions," Proceedings of the Atmospheric Refractivity Effects Assessment Conference, 23-25 January 1979, San Diego, CA. NOSC TD 260, pp 61-67.
- Trebits, B., M. Horst, M. Long, N. Currie and J. Peifer, "Millimeter Radar Sea Return Study," Georgia Institute of Technology, Project A-2013, Interim Report, July 1978.

